Dalton Transactions

Solvent-Dependent Transition from Concerted Electron-Proton to Proton Transfer in Photoinduced Reactions between Phenols and Polypyridine Ru Complexes with Proton-Accepting Sites

Journal:	*Dalton Transactions*
Manuscript ID	DT-ART-09-2018-003858.R1
Article Type:	Paper
Date Submitted by the Author:	17-Oct-2018
Complete List of Authors:	Lymar, Sergei; Brookhaven National Laboratory, Chemistry Ertem, Mehmed Z.; Brookhaven National Laboratory, Chemistry Department Polyansky, Dmitry; Brookhaven National Laboratory, Chemistry

Solvent-Dependent Transition from Concerted Electron-Proton to Proton Transfer in Photoinduced Reactions between Phenols and Polypyridine Ru Complexes with Proton-Accepting Sites

Sergei V. Lymar,* Mehmed Z. Ertem, and Dmitry E. Polyansky*
Chemistry Division, Brookhaven National Laboratory, Upton, New York 11973-5000, U.S.A.

Abstract. The bimolecular rate coefficients (k_q^{obs}) for quenching the metal-to-ligand charge transfer excited states of two Ru polypyridine complexes containing H-bond accepting sites by six *p*-substituted phenols exhibit abrupt deviations from the expected linear correlations of $logk_q^{obs}$ with phenol's Hammett σ_p constant. This pattern is attributed to a transition of the quenching mechanism from a concerted electron-proton transfer (EPT) to a proton transfer (PT); the latter becomes predominant for the most acidic phenols in MeCN, but not in CH_2Cl_2. This assertion is supported by a detailed thermochemical analysis, which also excludes the quenching pathways involving electron transfer from phenols with or without deprotonation of phenols to the solvent, either concerted or sequential. The transition from EPT to PT upon the σ_p increase is consistent/supported by the magnitudes of the measured and computed PhOH/OD kinetic isotope effects and by the observed reduction of the EPT product yields upon replacing the low σ_p methoxyphenol by the high σ_p nitrophenol. In addition to modulating the relative contribution of the EPT and PT quenching pathways, the solvent strongly affects the bimolecular rate coefficients for the EPT quenching proper. Unlike with H-atom transfer reactions, this kinetic solvent effect could not be quantitatively accounted for by the phenol-solvent H-bonding alone, which suggests a solvent effect on the H-bonding constants in the phenol-Ru complex precursor exciplexes and/or on the unimolecular EPT rate coefficients within these exciplexes.

Introduction

Concerted electron-proton transfer (EPT) in general and its photoinduced variety in particular are of growing interest due to their involvement in redox catalysis and charge separation and transport, and the substantial body of work on EPT reactions has been summarized in several recent reviews.[1-10] While hydrogen bonding between the proton donating and accepting reactant sites is widely recognized as a prerequisite to EPT, we have previously shown that accounting for the H-bonding of comparable strength between these reactants and solvent is essential for the meaningful kinetic analysis of the photoinduced EPT reactions.[11] However, previous studies of these reactions were typically confined to a single solvent and commonly ignored the reactant-solvent interactions.[12-15] One notable exception involves an H-atom transfer (HAT), a special case of EPT, whereby both electron and proton are transferred between the same pair of atoms. In a series of papers, Ingold and co-workers[16-18] have demonstrated that the observed solvent effect on the bimolecular rate constant of HAT can be quantitatively accounted for by considering the donor's H-bonding to solvent. Specifically, they suggested that this H-bonding renders the donor completely unreactive toward an H-atom acceptor.

Chart 1. Ruthenium complexes containing the proton-accepting, uncoordinated, ligand's **N** sites investigated in this work (bpy = 2,2′-bipyridine; pbn = 2-(2-pyridyl)benzo[*b*]-1,5-naphthyridine; bpz = 2,2′-bipyrazine).

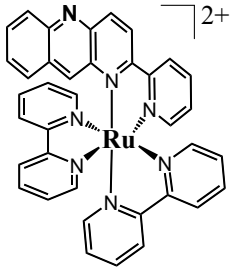

1 = $Ru(bpy)_2(pbn)^{2+}$

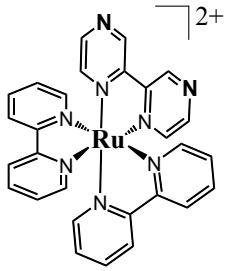

2 = $Ru(bpy)_2(bpz)^{2+}$

In a preceding paper[11] we extended Ingold's idea to propose a mechanistic model for describing the reactivity, including EPT, of a photo-excited metallocomplex containing H-bond accepting sites, such as Ru complexes **1** and **2** depicted in Chart 1, with an H-bond donating solute. In addition to the H-bonding between reactants and attendant physical and chemical quenching, this model accounts for the H-bonding of both reactants to solvent, as shown in Scheme 1, and its

implications have been corroborated by data on the reactivity of a triplet MLCT-excited complex **1** toward phenolic electron-proton donors.

In the present work, we expand that study to include complex **2** (Chart 1) whose triplet excited state, **2**(T), is less proton-accepting but more strongly oxidizing than **1**(T). In addition to determining the rate coefficients for triplet quenching in dichloromethane (CH_2Cl_2) and acetonitrile (MeCN) by a series of *para*-substituted phenols covering a large range of Hammett substituent constants, we measure and interpret both the OH/OD kinetic isotope effect (KIE) and kinetic solvent effect (KSE). While for many reaction types the latter has been extensively studied,[19] there are hardly any literature data so far on the KSE for concerted EPT processes. In addition to modulating rate, solvents can alter both the mechanism and end products of a reaction between the same reactants. Herein, we report the first example of a solvent effect where the quenching through EPT that prevails in CH_2Cl_2 is replaced by proton transfer in MeCN. To aid in discriminating between these and other quenching pathways, we present a detailed analysis of the quenching energetics and the data on the reaction end products.

Scheme 1. General mechanism of a photochemical reaction between metallocomplexes (**X**; *e.g.*, **1** or **2** in Chart 1) containing an uncoordinated ligand's N-atom (**N**) and phenols in MeCN, invoking the complex-phenol ($K_{X\text{-}P}$), complex-solvent ($K_{X\text{-}S}$), and phenol-solvent ($K_{P\text{-}S}$) H-bonding pre-equilibria.[a]

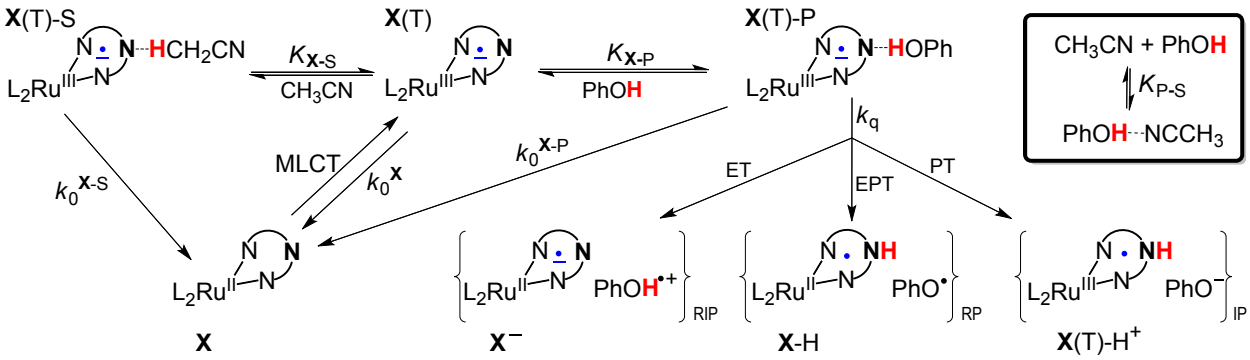

[a]**X**(T) denotes the triplet (excited MLCT) state, PhOH stands for a generalized reactive phenolic functionality, and RIP, RP, and IP subscripts indicate products in the form of a radical-ion, radical, and ion pair, respectively. The formal charge on **X** is +2.

Materials and Methods

Solvents (≥99.9% pure), phenols (all > 97% purity), and 2,2,2-trifluoroethanol (TFE, CF_3CH_2OH and CF_3CH_2OD, ≥99% pure) were obtained from Sigma-Aldrich. TFE was used as received. Acetonitrile was distilled from potassium borohydride and dichloromethane was passed through activated neutral alumina, upon which both solvents were dried over activated 3Å molecular sieves. Phenols were purified by sublimation. Their O-deuteration was carried out by the H/D exchange in CH_3OD followed by its vacuum removal, which gave a greater than 98% deuterium enrichment per NMR in CD_3CN. Ruthenium complexes were prepared according to the literature procedures: $[Ru(bpy)_2(pbn)](PF_6)_2$,[20] and $[Ru(bpy)_2(bpz)][PF_6]_2$.[21]

All samples were prepared and transferred into an airtight 1 cm path-length optical cuvette inside an inert atmosphere glovebox. Transient absorption and emission were measured at 25 °C using a home-built flash photolysis system,[22] with excitation provided either by 532 nm, ~2 ns pulses from a Nd/YAG laser (SpectraPhysics Lab 170) or a tunable OPO (VersaScan/240/ULD) pumped by the 354.7 nm output of the Lab 170. The excitation energy was maintained in the 4-7 mJ/pulse range. A pulsed Xe-arc lamp was used as the analyzing light source. Either a PMT (Hamamatsu, R928) or gated intensified CCD (Princeton Instruments, PI-MAX 1024UNIGEN2) was used as a detector. Sample integrity during a transient experiment was routinely tested by comparing its before-and-after UV/vis spectra measured with an Agilent 8453 spectrophotometer.

Molecular structures were optimized at the M06 level of density functional theory[23-25] with the SMD continuum solvation model[26] and the Stuttgart [8s7p6d2f | 6s5p3d2f] ECP28MWB contracted pseudopotential basis set[27] on Ru and the 6-31G(d) basis set on all other atoms.[28] Non-analytical integrals were evaluated using the integral=grid=ultrafine option, as implemented in Gaussian 09 software.[29] The nature of all stationary points was verified by analytic computation of vibrational frequencies that were also used for computing the zero-point vibrational energies and molecular partition functions. The latter were used for evaluating the 298 K thermal free energy contributions under the usual ideal-gas, rigid-rotator, harmonic oscillator approximation.[30] To arrive at the final, composite free energies that are reported for a 1 M solute standard state, these contributions were added to the single-point, SMD-solvated M06 electronic energies computed at the optimized geometries obtained with the initial basis using the def2-TZVPP basis

set on Ru and the def2-TZVP basis set[31] on all other atoms. Further computational details concerning the kinetic isotope effect calculations are given in SI section S5.

Results and Discussion

Quenching kinetics. The observed lifetimes of the emission decay kinetics of **1**(T) and **2**(T) at various concentrations of added phenols were converted to Stern-Volmer plots (SI section S1) and analyzed in terms of the reaction mechanism shown in Scheme 1. Recently, we have shown[11] that, provided all H-bonding equilibria involved are rapid relative to all other excited state processes, this mechanism leads to the following Stern-Volmer expression for the observed emission rate coefficient (k_{obs}) and lifetime (τ_{obs}),

$$\frac{k_{\mathrm{obs}}}{k_0} = \frac{\tau_0}{\tau_{\mathrm{obs}}} = 1 + \frac{\tau_0\left(k_{\mathrm{q}} + k_0^{\mathrm{X\text{-}P}} - k_0\right)K_{\mathrm{X\text{-}P}}^{\mathrm{app}}[\mathrm{P}]_0}{1 + K_{\mathrm{X\text{-}P}}^{\mathrm{app}}[\mathrm{P}]_0} = 1 + \frac{\tau_0 k_{\mathrm{q}}^{\mathrm{app}} K_{\mathrm{X\text{-}P}}^{\mathrm{app}}[\mathrm{P}]_0}{1 + K_{\mathrm{X\text{-}P}}^{\mathrm{app}}[\mathrm{P}]_0} \qquad (1)$$

where $k_0 = \left(k_0^{\mathrm{X}} + k_0^{\mathrm{X\text{-}S}}K_{\mathrm{X\text{-}S}}\right)/(1 + K_{\mathrm{X\text{-}S}})$ and $\tau_0 = {}^1\!/_{k_0}$ are the decay rate constant and lifetime measured in the absence of phenol, $[\mathrm{P}]_0$ is the analytical concentration of added phenol, $k_0^{\mathrm{X\text{-}P}}$ is the natural decay rate constant of the **X**(T)-P exciplex (in the absence of reactive quenching, when $k_{\mathrm{q}} = 0$, and **X**(T)-P decays only by a non-radiative transition and emission), $k_{\mathrm{q}}^{\mathrm{app}} = k_{\mathrm{q}} + k_0^{\mathrm{X\text{-}P}} - k_0$ is the apparent unimolecular quenching rate coefficient, and $K_{\mathrm{X\text{-}P}}^{\mathrm{app}}$ is the apparent equilibrium constant of the H-bonded **X**(T)-P exciplex formation; that is,

$$K_{\mathrm{X\text{-}P}}^{\mathrm{app}} = \frac{K_{\mathrm{X\text{-}P}}}{(1 + K_{\mathrm{P\text{-}S}})(1 + K_{\mathrm{X\text{-}S}})} \qquad (2)$$

In this equation, the constituent equilibrium constants for the H-bonded phenol-solvent (P-S) species and **X**(T)-S and **X**(T)-P exciplexes are defined through the concentrations of unbound **X**(T) complex and phenol; that is, $K_{\mathrm{P\text{-}S}} = [\mathrm{P\text{-}S}]/[\mathrm{P}]$, $K_{\mathrm{X\text{-}S}} = [\mathbf{X}(\mathrm{T})\text{-}\mathrm{S}]/[\mathbf{X}(\mathrm{T})]$, and $K_{\mathrm{X\text{-}P}} = [\mathbf{X}(\mathrm{T})\text{-}\mathrm{P}]/([\mathbf{X}(\mathrm{T})][\mathrm{P}])$. All equilibrium and rate parameters in eqs. 1 and 2 are generally solvent-dependent.

The quenching measurements of both **1**(T) and **2**(T) gave linear Stern-Volmer plots for all phenols (SI section S1) indicating that in all cases the $K_{\mathrm{X\text{-}P}}^{\mathrm{app}}[\mathrm{P}]_0$ product is much smaller than unity in the accessible phenol concentration range, and eq. 1 reduces to

$$\frac{k_{\mathrm{obs}}}{k_0} = \frac{\tau_0}{\tau_{\mathrm{obs}}} = 1 + \tau_0 k_{\mathrm{q}}^{\mathrm{app}} K_{\mathrm{X\text{-}P}}^{\mathrm{app}}[\mathrm{P}]_0 = 1 + \tau_0 k_{\mathrm{q}}^{\mathrm{obs}}[\mathrm{P}]_0 \qquad (3)$$

where

$$k_{\mathrm{q}}^{\mathrm{obs}} = k_{\mathrm{q}}^{\mathrm{app}} K_{\mathrm{X\text{-}P}}^{\mathrm{app}} = \left(k_{\mathrm{q}} + k_0^{\mathrm{X\text{-}P}} - k_0\right)K_{\mathrm{X\text{-}P}}^{\mathrm{app}} \qquad (4)$$

is the observed bimolecular quenching rate coefficient obtainable from the slope of a Stern-Volmer plot. These rate coefficients are summarized in Table 1. It is clear from eqs 1, 3, and 4 that: (1)

accurate separation of $k_q + k_0^{X\text{-}P}$ from $K_{X\text{-}P}^{app}$ in k_q^{obs} requires data in the $K_{X\text{-}P}^{app}[P]_0 \gg 1$ region, where the Stern-Volmer dependencies approach a plateau, and (2) even when $K_{X\text{-}P}^{app}$ can be evaluated, it is generally impossible to distinguish between the chemical (k_q) and physical ($k_0^{X\text{-}P}$) quenching from the emission quenching data alone.

Table 1. Bimolecular rate coefficients (k_q^{obs} in 10^7 M^{-1} s^{-1}, eqs 3 and 4) for reactions between complexes **1**(T) and **2**(T) with *p*-substituted phenols obtained through transient emission measurements in MeCN and CH_2Cl_2.

Substituent (σ_p)[a]	Complex **1**(T)			Complex **2**(T)		
	k_q^{obs},[b] (KIE[c])		KSE[d]	k_q^{obs}, (KIE[c])		KSE[d]
	MeCN	CH_2Cl_2		MeCN	CH_2Cl_2	
MeO- (–0.27)	3.3	130 (4.0)	39	2.3	150 (2.0)	65
Ph- (–0.01)	1.4	44 (2.9)	31	0.92	42 (*2.1*)	46
Cl- (0.23)	0.43	12	28	0.20	6.0	30
MeOC(O)- (0.45)	0.28	4.6	16	0.093	2.0	22
NC- (0.66)	0.48	3.8 (1.6)	7.9	0.098	1.3 (2.4)	13
O_2N- (0.78)	0.88	2.4 (2.0)	2.7	0.16	1.2 (2.5)	7.8

[a]Hammett σ_p constants are from ref.[32]; [b]k_q^{obs} for **1**(T) are from ref.[11]; [c]Kinetic isotope effect, KIE = k_q^{obs}(PhOH)/k_q^{obs}(PhOD); [d]Kinetic solvent effect, KSE = $k_q^{obs}(CH_2Cl_2)/k_q^{obs}$(MeCN).

Recently, we have reasoned that the solvent-phenol H-bonding constant can be evaluated using Abraham HB acidity of the phenol donor (α_2^H) and HB basicity of the solvent acceptor (β_2^H), which leads to the following expression for $K_{P\text{-}S}$

$$logK_{P\text{-}S} = 7.354\alpha_2^H(\text{PhOH})\beta_2^H(S) + log[S] - 1.094 \qquad (5)$$

where $\alpha_2^H(\text{PhOH})$ is phenol's HB acidity, $\beta_2^H(S)$ is solvent's HB basicity, and [S] is solvent molar concentration.[11] The estimates obtained through eq. 5 and presented in Table 2 show that the magnitudes of the $1 + K_{P\text{-}S}$ factor in eq. 2 are large enough, particularly in MeCN, to make $K_{X\text{-}P}^{app}$ signicanly smaller than $K_{X\text{-}P}$, which undoubtedly contributes to the difficulty observing saturation in the Stern-Volmer dependencies predicted by eq. 1. In contrast, both MeCN and CH_2Cl_2 solvents

are very weak HB donors compared to phenols (Table 2), and we should expect only a small or negligible contribution to $K_{X\text{-}P}^{app}$ from the $1 + K_{X\text{-}S}$ factor.[11]

Energetics and mechanism of chemical quenching. Three mechanistic alternatives for chemical quenching are shown in Scheme 1 and include ET, PT or EPT reactions. The likelihood of the electron transfer (ET) pathway leading to the $\{\mathbf{X}^{-}/\mathrm{PhOH}^{\bullet+}\}_{RIP}$ radical-ion pair is governed by the relative reduction potentials of **X**(T) and $\mathrm{PhOH}^{\bullet+}$. The EPT pathway, whereby an electron is transferred to the Ru center and the proton is accepted by the ligand's N atom, generates the $\{\mathbf{X}\text{-H}/\mathrm{PhO}^{\bullet}\}_{RP}$ radical pair and relies on the difference between the N-H bond dissociation free energy (BDFE) in **X**(T)-H and BDFE of O-H in PhOH. The feasibility of the proton transfer (PT) pathway yielding the $\{\mathbf{X}(\mathrm{T})\text{-}\mathrm{H}^{+}/\mathrm{PhO}^{-}\}_{IP}$ ion pair depends on the relative pK_as of **X**(T)-H^{+} and phenol. We will now attempt to discriminate among these pathways by considering their energetics.

Table 2. BDFE of the O-H bond (kcal/mol), Brønsted acidities, and reduction potentials of *p*-substituted phenols in gas phase, MeCN, and CH_2Cl_2.[a]

Substituent (α_2^H)	Gas phase		MeCN (C_G = 52.6 kcal/mol)[b] $\alpha_2^H = 0.09$; $\beta_2^H = 0.44$				CH_2Cl_2 $\alpha_2^H = 0.13$; $\beta_2^H = 0.05$	
	BDE[c]	BDFE[d]	$K_{P\text{-}S}$	BDFE[e]	pK_a (PhOH)	E^0 ($PhO^{\bullet/-}$)[f]	$K_{P\text{-}S}$	BDFE[e]
MeO- (0.573)	84.2 ± 1.6	76.0	110	81.3	29.2[g]	–0.48	2.0	79.6
Ph- (0.595)	86.7 ± 1.7	78.5	130	83.9	27.2[g]	–0.25	2.1	82.1
Cl- (0.670)	90.7 ± 2.1	82.5	230	88.2	25.4[33]	0.04	2.2	86.1
NC- (0.787)	93.0 ± 1.8	84.8	540	91.1	22.7[34]	0.32	2.4	88.5
O_2N- (0.824)	93.9 ± 1.6	85.7	710	92.1	20.9[34]	0.48	2.5	89.4

[a]At 25 °C. Values of α_2^H and β_2^H are due to Abraham and co-workers.[35-37] An expanded version of this table is presented in SI section S2; [b]See SI section S2 for the C_G derivation; [c]Averages from Luo's compilation;[38] [d]Computed from eq S2.2 in SI section S2; [e]Estimated from the gas phase values using eq S2.25 in SI section S2; [f]Derived using eq 6 in V vs $Fc^{+/0}$; [g]Estimated from pK_a in DMSO (see Table S2.3 for details).

The gas-phase O-H bond dissociation energies (BDE) for phenols used in this work are known within ~1.8 kcal/mol, which allows evaluation of their BDFEs in both gas phase and solution

(Table 2; see SI section S2 for details). The latter relate to the acidities and reduction potentials of phenol and its radical-cation through the following equation (SI section S2),

$$\text{BDFE} - C_G = aE^0(\text{PhO}^{\bullet/-}) + b\text{p}K_a(\text{PhOH}) = aE^0(\text{PhOH}^{\bullet+/0}) + b\text{p}K(\text{PhOH}^{\bullet+}) \quad (6)$$

where a = 23.06 kcal/(mol V) and b = 1.364 kcal/mol serve to bring E^0 and pK_a into the kcal/mol scale, and C_G is a constant that depends only on temperature, solvent, and the choices of reference electrode and standard states. The reduction potentials of phenoxyl radical estimated through eq. 6 are included in Table 2. Notably, the C_G value that we have derived for MeCN (and several other solvents, including water) is in a non-trivial variance with its counterpart recommended by Mayer and co-workers;[8] the reasons for this disagreement are discussed in SI section S2.

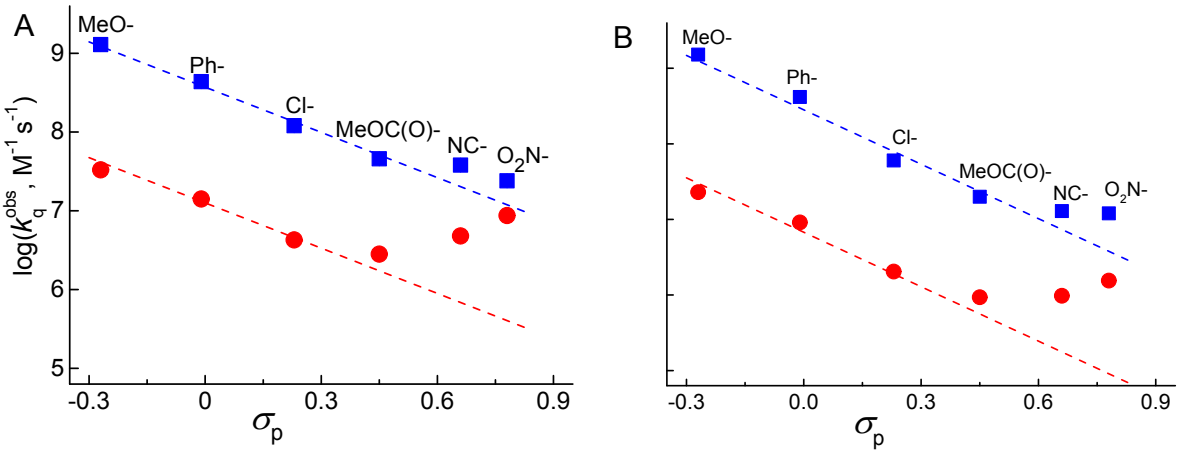

Figure 1. Hammett σ_p correlations of the apparent second-order rate coefficient k_q^{obs} (eq. 4) in CH_2Cl_2 (blue squares) and MeCN (red circles): for complex **1** (A) and for complex **2** (B). The parallel dashed lines with slopes of –1.9 (A) and –2.4 (B) serve as a visual aid for nonlinearity.

All relevant thermochemical properties of phenols (O-H BDFE, $E^0(\text{PhO}^{\bullet/-})$, and p$K_a$), as well as their HB acidity, exhibit linear correlations with Hammett σ_p (Figures S2.1-S2.3). These observations bode well for using the σ_p constant as a descriptor for the rate-free energy correlations in reactions of a common ET, PT, or EPT acceptor with various phenolic donors. As shown in Figure 1, for both Ru complexes the $logk_q^{obs}$ vs σ_p plots display reasonable linearity for the less acidic phenols with essentially the same slopes in MeCN and CH_2Cl_2, but significant positive deviations are apparent for the more acidic phenols. These deviations are especially conspicuous

in MeCN and for phenols with the strongest electron-withdrawing cyano- and nitro- substituents. We deem this pattern to be indicative of a modification of the reaction mechanism and suggest that the **X**(T) emission quenching occurs mainly through the EPT pathway for the less acidic phenols, but when the substituents become sufficiently electron-withdrawing, a contribution from the PT pathway becomes significant or even prevailing.

To examine this conjecture, we have used quantum chemical methods to compute the overall standard free energy changes in the EPT, PT, and ET reactions for fully separated reactants and products; that is,

$$\mathbf{X}(\mathrm{T}) + \mathrm{PhOH} = \mathbf{X}\text{-H} + \mathrm{PhO}^{\bullet} \qquad \Delta_{\mathrm{EPT}}G^0 \qquad (7)$$

$$\mathbf{X}(\mathrm{T}) + \mathrm{PhOH} = \mathbf{X}(\mathrm{T})\text{-H}^{+} + \mathrm{PhO}^{-} \qquad \Delta_{\mathrm{PT}}G^0 \qquad (8)$$

$$\mathbf{X}(\mathrm{T}) + \mathrm{PhOH} = \mathbf{X}^{-} + \mathrm{PhOH}^{\bullet+} \qquad \Delta_{\mathrm{ET}}G^0 \qquad (9)$$

Due to the lack of reliable experimental data, assessing the absolute accuracy of these computational results summarized in Table S3.1 is problematic. However, the internal consistency and relative accuracy of the computations can be evaluated by comparing with the available experiment-based data. These comparisons suggest that our calculated relative $\Delta_{\mathrm{EPT}}G^0$, $\Delta_{\mathrm{PT}}G^0$, and $\Delta_{\mathrm{ET}}G^0$ for reactions of various phenols with the same **X**(T) and for reactions of the same phenol with **1**(T) and **2**(T) are, on average, within ~2 kcal/mol of the actual values (Tables S3.2 and S3.3).

Because the nascent products of ET and PT are not separated, but rather emerge as ion pairs (Scheme 1), the computed free energies of ET and PT reactions must be corrected for the free energy of ion pairing ($\Delta_{\mathrm{IP}}G$) before comparing them with $\Delta_{\mathrm{EPT}}G^0$, which requires no electrostatic correction. Using a model suggested by Fuoss,[39] we estimate $\Delta_{\mathrm{IP}}G$ as 4.2 and −13.6 kcal/mol for the ET and PT products, respectively, in CH_2Cl_2. In MeCN, the corresponding $\Delta_{\mathrm{IP}}G$ are smaller, 0.9 and −3.6 kcal/mol (Table S3.5).

These corrected free energies ($\Delta_{\mathrm{PT}}G' = \Delta_{\mathrm{PT}}G^0 + \Delta_{\mathrm{IP}}G$ and $\Delta_{\mathrm{ET}}G' = \Delta_{\mathrm{ET}}G^0 + \Delta_{\mathrm{IP}}G$) along with $\Delta_{\mathrm{EPT}}G^0$ are compiled in Table 3, and their relative magnitudes are plotted in Figure 2. These plots suggest that the EPT pathway for both **1**(T) and **2**(T) should be more favorable than the other two pathways in both solvents and for all phenols. The free energy gaps between ET and EPT is within 15-25 kcal/mol for the most readily oxidizable *p*-MeOPhOH and linearly increase with σ_{p} to over 35 kcal/mol. It is, thus, improbable that the ET pathway can compete with EPT or even appreciably

contribute to the chemical quenching of **X**(T). This assertion is supported by: (i) the substantial OH/OD kinetic isotope effect (Table 1), and (ii) our previously reported observation[11] that a structural isomer of **1**(T) with a nearly identical reduction potential is completely unreactive toward phenols because it cannot engage in EPT or PT due to its sterically screened proton-accepting nitrogen site (Chart S4.1 and Table S3.4). This conclusion is consistent with the reactivity of **2**(T) toward hydroquinone that was previously assigned to a concerted EPT process.[12]

Table 3. Computed free energy changes (kcal/mol) for EPT, PT, and ET reactions of **1**(T) with p-substituted phenols leading to the $\{\mathbf{1}\text{-H}/\text{PhO}^{\bullet}\}_{RP}$, $\{\mathbf{1}(T)\text{-H}^{+}/\text{PhO}^{-}\}_{IP}$, and $\{\mathbf{1}^{-}/\text{PhOH}^{\bullet+}\}_{RIP}$ contact pair, respectively (Scheme 1). For the corresponding reactions of **2**(T): all $\Delta_{EPT}G'$ are larger by 3.4 in MeCN and 4.1 in CH_2Cl_2; all $\Delta_{PT}G'$ are larger by 6.6 in MeCN and 7.3 in CH_2Cl_2; all $\Delta_{ET}G'$ are smaller by 2.1 in MeCN and 3.0 in CH_2Cl_2.

Substituent	MeCN[a]			CH_2Cl_2[b]		
	$\Delta_{EPT}G^0$	$\Delta_{PT}G'$	$\Delta_{ET}G'$	$\Delta_{EPT}G^0$	$\Delta_{PT}G'$	$\Delta_{ET}G'$
MeO-	–11.9	16.0	11.6	–14.0	21.8	10.3
Ph-	–8.9	11.3	16.6	–10.9	17.0	15.5
Cl-	–6.3	11.1	25.1	–8.5	16.4	24.4
MeOC(O)-	–3.0	7.3	30.9	–5.2	12.5	30.4
NC-	–2.1	4.9	34.2	–4.4	9.6	34.0
O_2N-	–0.9	1.9	39.6	–2.9	6.3	38.9

[a]$\Delta_{PT}G' = \Delta_{PT}G^0 - 3.6$, and $\Delta_{ET}G' = \Delta_{ET}G^0 + 0.9$; [b]$\Delta_{PT}G' = \Delta_{PT}G^0 - 13.6$, and $\Delta_{ET}G' = \Delta_{ET}G^0 + 4.2$

In contrast, the initially large energy gaps between PT and EPT linearly decrease with σ_p and nearly close for the most acidic phenols in MeCN. This trend opens a possibility for a large contribution from PT to the overall chemical quenching of **X**(T), particularly since the usually adiabatic PT reactions involve much less nuclear reorganization and, in this sense, are far simpler than concerted EPT reactions. This inference supports our interpretation of non-linearity of the σ_p dependence in Figure 1; namely, the idea of the mechanistic transition from EPT to PT that occurs for phenols with strongly electron-withdrawing groups. This effect is particularly prominent in MeCN where the large deviation from linearity suggests that PT contribution to k_q^{obs} amounts to

~85% for cyanophenol and ~95% for nitrophenol. In CH_2Cl_2, the non-linearity is much smaller, barely noticeable. This observation is consistent with the computational prediction that EPT remains substantially more favorable than PT even for the most acidic phenols, which would strongly decrease the PT contribution to k_q^{obs}.

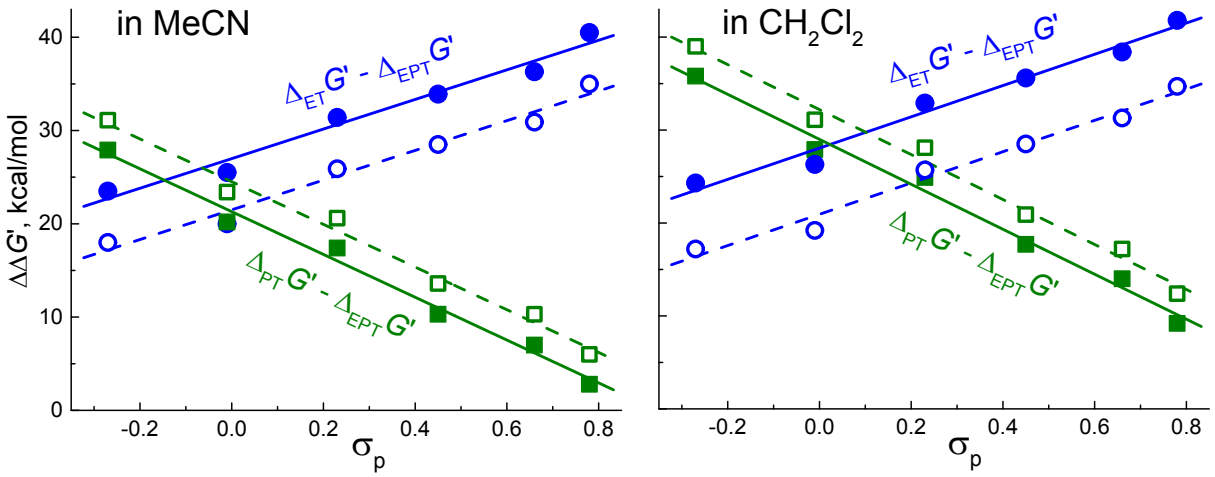

Figure 2. The σ_p dependencies of computed free energies corrected for the product ion-pairing for PT (squares) and ET (circles) reactions relative to $\Delta_{EPT}G^0$ ($\Delta\Delta G' = \Delta_{PT}G' - \Delta_{EPT}G^0$ and $\Delta\Delta G' = \Delta_{ET}G' - \Delta_{EPT}G^0$) between **1**(T) (solid symbols and lines) and **2**(T) (open symbols and dashed lines) and *p*-substituted phenols. The $\Delta G'$ values are taken from Table 3. The σ_p dependencies of computed $\Delta\Delta G^0$ uncorrected for the product ion-pairing are shown in Figure S3.1.

The difference in reactivity between low and high σ_p phenols is further contrasted by the computed adiabatic energy profiles along the N-H distance between the ligand's N atom of **1**(T) and the phenolic proton (r_{N-H}) in the **1**(T)-methoxyphenol and **1**(T)-nitrophenol H-bonded exciplexes (Figure S3.2). In both CH_2Cl_2 and MeCN, these profiles display early saddle points for *p*-methoxyphenol (r_{N-H} = ~1.6 Å) and late saddle points for *p*-nitrophenol (r_{N-H} ~1.2 Å), which is in line with the EPT driving force differences (Table 3). Spin population analysis (Table S3.6) reveals an electron transfer from a phenol to the Ru atom that occurs after passing through the saddle point in all cases (except for 1(T)-nitrophenol in MeCN), upon which further r_{N-H} decrease leading to the EPT products is accompanied by a sharp energy decrease (Figure S3.2). The

modifications of this reactivity pattern arising from the vibronic nonadiabaticity will be discussed below along with the kinetic isotope effects.

All our attempts to locate a transition state for PT within the **1**(T)-methoxyphenol H-bonded exciplex were unsuccessful in both solvents due to electron transfer occurring early on the reaction coordinate, as shown in computed adiabatic energy profiles (Figure S3.2) and spin population data (Table S3.6). Thus, for *p*-methoxyphenol, EPT is predicted to be the dominant pathway. In contrast, the PT transition states were located for the **1**(T)-nitrophenol exciplex, and the computed activation energies predict PT to be more facile in CH_3CN than in CH_2Cl_2 (Figure S3.3).

Besides the EPT, ET, and PT depicted in Scheme 1 and considered hitherto, two alternative chemical quenching pathways that involve an electron transfer to **X**(T) and a proton transfer to solvent can be envisioned, at least in the higher dielectric MeCN solvent (Scheme 2). One of these pathways consists of the PhOH acid dissociation pre-equilibrium and rapid oxidation of the PhO^- anion. This type of reactivity and its role in certain H-atom transfer reactions in MeCN have been discussed by Litwinienko and Ingold,[16, 40] who dubbed this pathway sequential proton-loss electron transfer (SPLET). Although oxidations of all PhO^- are energetically favorable for both **1**(T) and **2**(T) (by 3 to 28 kcal/mol, Table S4.1) and, therefore, can be rapid, the phenol pK_a's are undoubtedly much too high for SPLET to measurably contribute to the quenching rate coefficients of the order of 10^6–10^7 M^{-1} s^{-1} that we have observed.

Scheme 2. Alternative, solvent-assisted CPLET and SPLET pathways for **X**(T) quenching in MeCN.

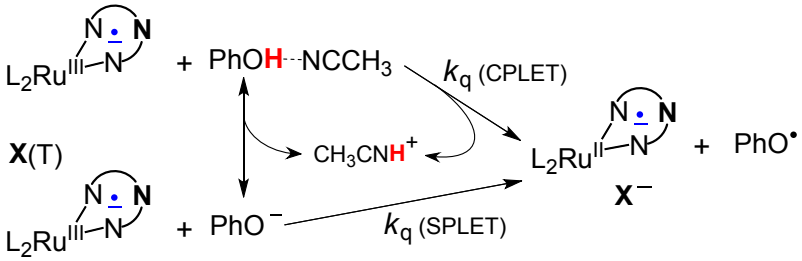

The other pathway in Scheme 2 amounts to a concerted proton-loss electron transfer (CPLET), whereby the electron goes to **X**(T) and the proton is accepted by solvent in a concerted manner. Although this mode of proton-coupled electron transfer has been reported,[41-46] we evaluate this

reaction to be prohibitively uphill (12 to 26 kcal/mol, Table S4.1) for both **1**(T) and **2**(T) with all phenols. In addition, the unavailability of both SPLET and CPLET pathways is strongly supported by our previous observation that a structural isomer of **1**(T) with nearly identical reduction potential but no proton accepting capability (Chart S4.1 and Table S3.4) is completely unreactive toward phenols in MeCN.[11] For the less basic CH_2Cl_2 solvent, these pathways are even less energetically feasible.

H/D kinetic isotope effect. Because k_q^{obs} is the product of the HB equilibrium constant $K_{X\text{-}P}^{app}$ and unimolecular quenching rate coefficient k_q^{app} (eq. 4), the significant KIE on k_q^{obs} that we observe (Table 1) may, in principle, be distributed between these constituent factors. Literature reports on the H/D isotope effect on hydrogen bonding of phenols are few,[47-52] and the data that have been obtained mainly through IR spectroscopic studies are conflicting. In their critical evaluation of this issue, Boettcher and Drago[49] have attributed these inconsistencies mostly to the difficulties and large errors associated with obtaining HB equilibrium constants from the O-H/O-D stretching frequency shifts. From their own calorimetric and IR measurements of phenol hydrogen bonding to various bases they concluded that no detectable H/D isotope effect is to be expected for the HB strengths in the 0 to 10 kcal/mol range. This conclusion is corroborated by a report of a less than 10% change of the phenols' H-bonding constants with vinyl acetate upon H/D substitution in the phenolic OH group.[51]

Previously, we have shown[11] that: (i) 2,2,2,-trifluoroethanol (TFE, $\alpha_2^H = 0.567$) can serve as a proxy for *p*-MeOPhOH ($\alpha_2^H = 0.573$) with respect to H-bonding with **1**(T), (ii) a Stern-Volmer plot for the **1**(T) quenching by TFE in CH_2Cl_2 exhibits a saturation behavior characteristic of **1**(T)-TFE H-bonding (eq. 1), from which the $K_{1\text{-}TFE}^{app}$ H-bonding constant could be determined, and (iii) the quenching is physical due to shortening the **1**(T) lifetime upon its H-bonding to TFE and does not involve EPT, PT, or ET. Due to relatively low quenching efficiencies of alcohols and typically higher solubilities as compared to similarly HB acidic phenols, the saturation of Stern-Volmer plots and attendant determination of the H-bonding constants can be more readily achieved with alcohols.[11] In contrast, only the beginning of Stern-Volmer saturation could so far be observed for the EPT reactions with phenols, which affords only crude H-bonding estimates.[13]

Here, we use 2,2,2,-trifluoroethanol to directly measure the H/D isotope effect on the H-bonding equilibrium in the **2**-TFE system. From the Stern-Volmer dependencies for quenching of **2**(T) by

OH and OD TFE in CH_2Cl_2 (Figure 3) we obtain $K^{app}_{\mathbf{2}\text{-TFE}}$(OH) = 1.52 ± 0.14 M^{-1} and $K^{app}_{\mathbf{2}\text{-TFE}}$(OD) = 1.60 ± 0.18 M^{-1} and conclude that the H-bonding constant is, within the experimental error, independent of the H/D isotopic substitution. Assuming that $K^{app}_{\mathbf{2}\text{-TFE}} \approx K^{app}_{\mathbf{2}\text{-MeOPhOH}}$, we estimate k_q^{app}(MeOPhOH)/k_q^{app}(TFE) = 520, which suggests that k_q^{app} for *p*-MeOPhOH is dominated by chemical quenching; that is, $k_q >> k_0^{2\text{-P}}$ and $k_q^{app} \approx k_q$ in eqs. 1 and 4. Thus, we ascribe the KIE on k_q^{obs} for *p*-MeOPhOH (and, by inference, for other phenols in Table 1) entirely to the rate constant of chemical quenching, k_q. This assignment implies that EPT and/or PT pathways involving proton/deuteron transfer dominate chemical quenching, but the isotope-insensitive ET pathway plays no role.

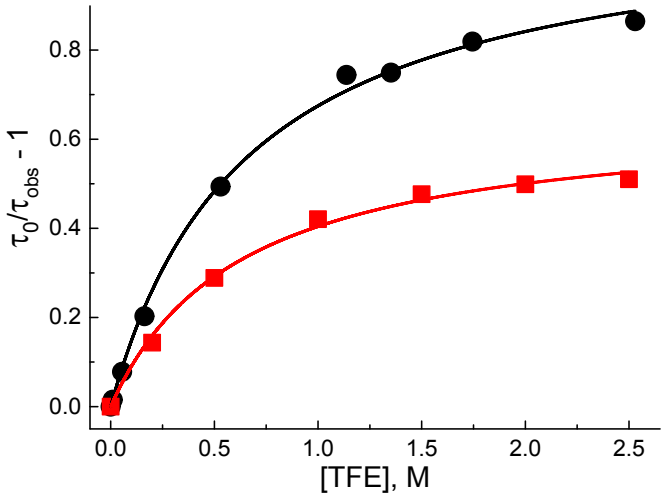

Figure 3. Stern-Volmer plots for quenching of **2**(T) by OH (circles) and OD (squares) TFE in CH_2Cl_2. Fits to the functional form of eq. 1 ($\tau_o/\tau_{obs} - 1 = \tau_0 k_q^{app} K^{app}_{\mathbf{2}\text{-TFE}}[TFE]/(1 + K^{app}_{\mathbf{2}\text{-TFE}}[TFE])$, solid curves) correspond to the apparent equilibrium constants for the formation of the **2**(T)-TFE H-bonded exciplex of $K^{app}_{\mathbf{2}\text{-TFE}}$(OH) = 1.52 ± 0.14 M^{-1} and $K^{app}_{\mathbf{2}\text{-TFE}}$(OD) = 1.60 ± 0.18 M^{-1}, which amounts to an isotope effect of 0.95 ± 0.14. The fitted k_q^{app}(OH) = (1.91 ± 0.22)×10^6 s^{-1} and k_q^{app} (OD) = (1.12 ± 0.12)×10^6 s^{-1} correspond to the lifetimes of the H-bonded **2**(T)-TFE exciplexes of $\tau_0^{2\text{-TFE}}$(OH) = 276 and $\tau_0^{2\text{-TFE}}$(OD) = 353 ns, which are 60 and 47%, respectively, shorter than the unbound **2**(T) lifetime.

The kinetic isotope effects have also been investigated using constrained DFT calculations[53] and the nonadiabatic EPT rate equations[54-60] for transitions between the reactant and product vibronic states, as detailed in SI section S5. These massive computations were limited to the **1**(T)-MeOPhOH and **1**(T)-O_2NPhOH exciplexes in CH_2Cl_2 and predicted KIE of 3.1 and 1.1, respectively, for the EPT reaction. Whereas the former value is in fair agreement with the experimentally determined KIE of 4.0, the latter value is much smaller than the measured KIE of 2.0 (Table 1). On the other hand, our computations for PT in the **1**(T)-O_2NPhOH exciplex yield a much larger KIE of 4.7 (see caption to Figure S3.3), and the predicted and observed KIE for **1**(T)-O_2NPhOH can be reconciled assuming ~25% contribution from PT to the overall chemical quenching. This assumption is in line with our proposal of the EPT-to-PT reactivity shifting with σ_p increase.

Transient absorption and products. The proposed shift of chemical quenching from EPT to PT upon σ_p increase implies a possibility for the attendant alteration of products and their yields (Scheme 3). The $\{$**X**-H/PhO$^{\bullet}\}_{RP}$ pair generated by EPT can undergo either thermodynamically favorable EPT from **X**-H back to PhO$^{\bullet}$ within the solvent cage with no net products formation or decompose to the separated **X**-H and PhO$^{\bullet}$ products. The fate of the $\{$**X**(T)-H^+/$PhO^-\}_{IP}$ pair produced by PT can be more complicated. Its decomposition can yield a mixture of **X**-H, PhO$^{\bullet}$, **X**(T)-H^+, and PhO^- as separated products, whose relative yields depend on the competition between the thermodynamically favorable and rapid intra-pair electron transfer, triplet deactivation, and diffusional separation. These expectations have been investigated by transient absorption spectroscopy of *p*-methoxy- and *p*-nitrophenol with complex **1**. The latter has been selected because a spectrum of its EPT product, **1**-H, is available from a prior pulse radiolysis study (Figure S6.1).[61]

Scheme 3. Competing pathways leading to separated products following EPT and PT reactions in the H-bonded **X**(T)-P exciplex.

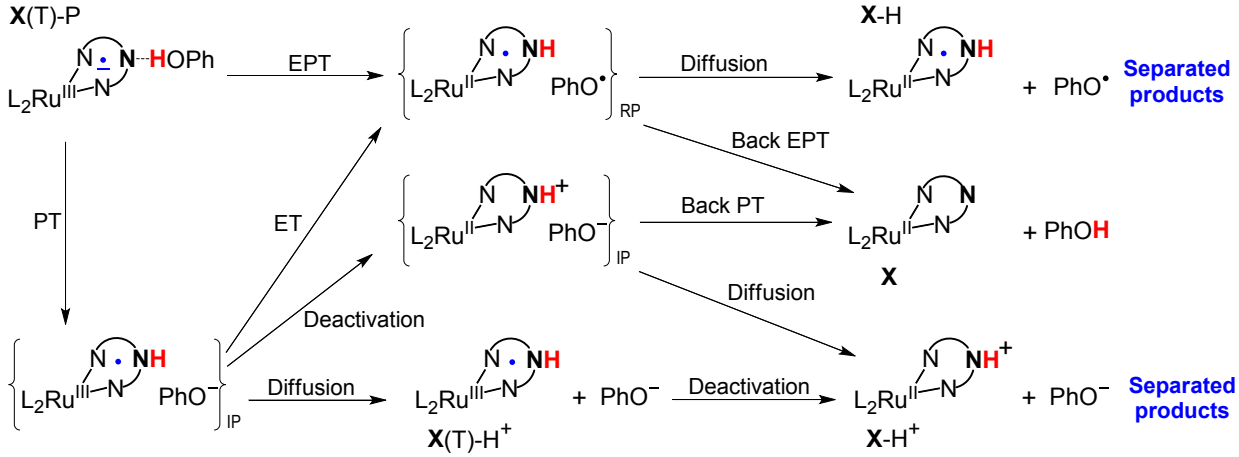

The primary spectra-kinetic flash photolysis data are presented in Figure S6.2, and the absorption spectra recorded upon the completion of **1**(T) quenching are compared in Figure 4. For the **1** + *p*-MeOPhOH system in both MeCN and CH_2Cl_2, these spectra show a prominent *p*-MeOPhO• band around 400 nm and a good match to the **1**-H – **1** difference spectrum above 450 nm. The latter observations strongly suggest that **1**-H and *p*-MeOPhO• are the predominant products, as would be expected for quenching through EPT. When going to *p*-O_2NPhOH, the correspondence between the product spectrum above 450 nm and that of **1**-H remains good in CH_2Cl_2, but the agreement becomes rather poor in MeCN. In this case, the product spectrum is better explained by a superposition of the **1**-H and **1**-H^+ spectra with approximately equal weights, which is consistent with a contribution from the PT quenching pathway.

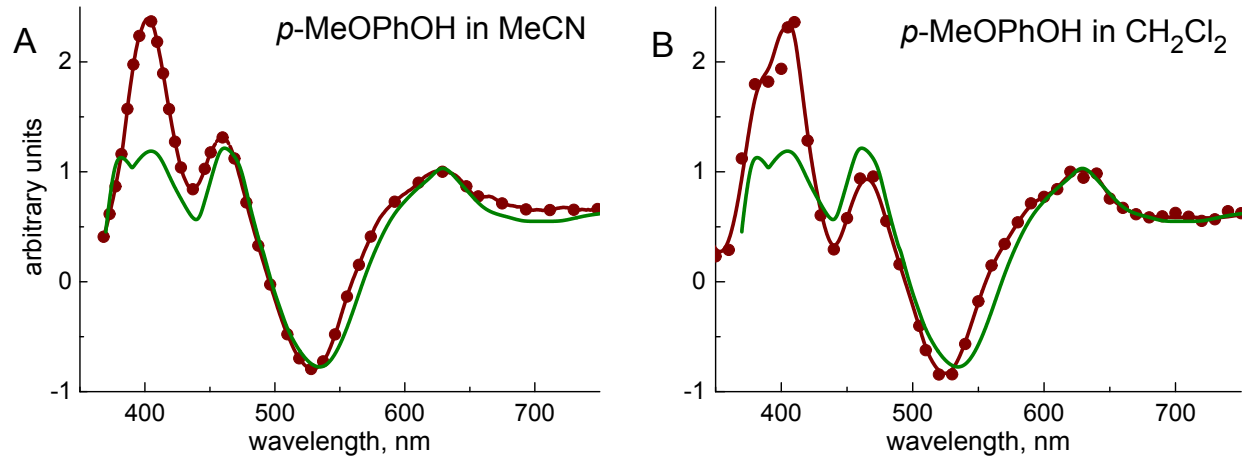

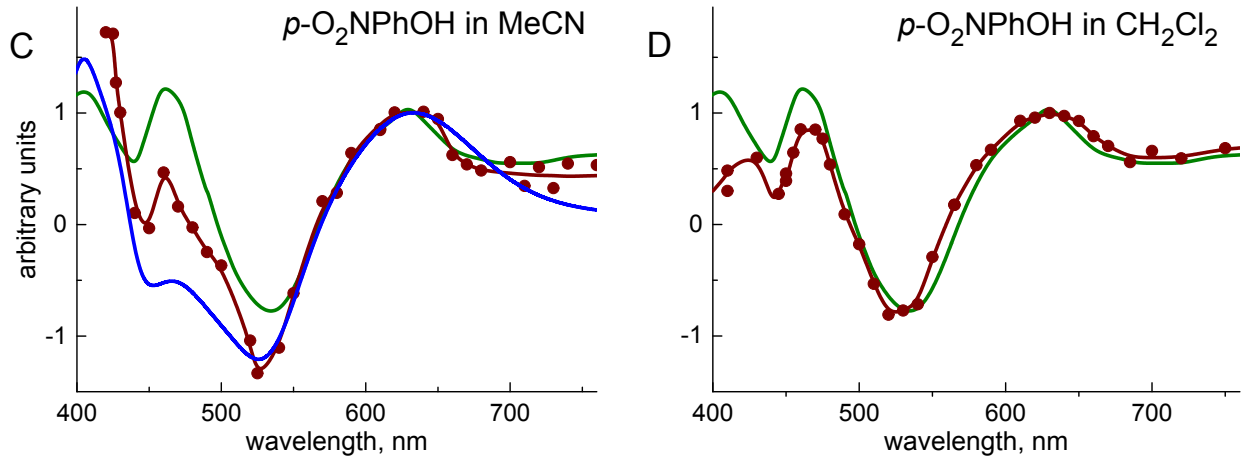

Figure 4. Overlays of the independently measured (Figure S6.1) difference spectra **1**-H – **1** (green line), **1**-H^+ – **1** (blue line), and spectra observed after the **1**(T) quenching completion (wine symbols and lines). The latter have been recorded under conditions of comparable **1**(T) yields and quenching efficiencies and correspond to the difference between absorption by the separated products and that of **1**. To facilitate direct comparison, all spectra are normalized at 628 nm, where **1**-H and **1**-H^+ exhibit nearly equal molar absorptivity. The intense absorption band around 400 nm in A and B contains a contribution from the MeOPhO$^\bullet$ radical.[62] See Figure S6.2 for the primary spectra-kinetic data.

For comparing the combined yields of **1**-H + **1**-H^+ products from the **1**(T) quenching by *p*-methoxy- and *p*-nitrophenol, the absorption spectra recorded upon the completion of quenching have been normalized to both the amount of **1**(T) created by flash photolysis and the quenching efficiency. The resulting spectra in Figure 5 reflect the relative compositions and yields of separated products originating from the same aggregate amount of nascent $\{$**1**-H/PhO$^\bullet\}_{RP}$ + $\{$**1**(T)-H^+/$PhO^-\}_{IP}$ pairs. It is immediately obvious from comparing the black and red spectra in this figure that the combined yield of the **1**-H and **1**-H^+ products markedly decreases on going from methoxy- to nitrophenol. This decrease amounts to ~90% in MeCN, and ~40% in CH_2Cl_2, as has been estimated from the spectra amplitudes at 628 nm (where **1**-H and **1**-H^+ exhibit virtually equal molar absorptivity; Figure S6.1).

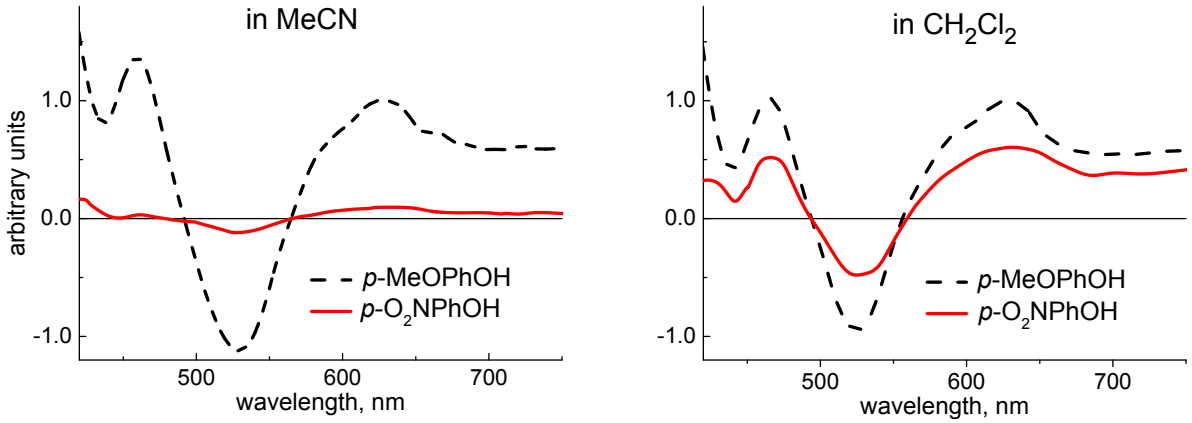

Figure 5. Final transient spectra from Figure S6.2 normalized to the amount of **1**(T) created by flash photolysis and chemical quenching efficiency (see SI section S6 for the procedure). At wavelengths longer than 500 nm, these spectra are exclusively due to conversion of **1** into the **1**-H and **1**-H^+ separated products.

A large decrease of product yield in MeCN is consistent with the shift of quenching pathway from predominantly EPT to mainly PT provided the $\{$**1**(T)-H^+/$PhO^-\}_{IP}$ pair decays primarily through deactivation followed by back PT yielding no net products (Scheme 3). This scenario is entirely plausible, for dramatic lifetime decreases of triplet excited states upon protonation have been observed for a number of Ru complexes analogous to **1** and containing heteroaromatic ligands with uncoordinated nitrogen.[63-65] A highly exoergic back proton transfer in $\{$**1**-H^+/$PhO^-\}_{IP}$ should also be sufficiently rapid to compete with diffusional decomposition of this electrostatically bound ion pair. A smaller decrease of the separated product yield on replacing *p*-methoxy- by *p*-nitrophenol in CH_2Cl_2 than in MeCN is consistent with the smaller contribution from the PT quenching pathway in CH_2Cl_2 and attendant smaller deviations from linearity of the Hammett σ_p correlation in Figure 1; we estimate that EPT is still responsible for ~60% of the **1**(T) + *p*-O_2NPhOH reaction. Thus, we interpret the transient absorption data as further supporting the transition of quenching mechanism from EPT to PT with the increase of electron-withdrawing power of the phenol's *p*-substituent. This transition is significantly more prominent in MeCN than in CH_2Cl_2, which is, we believe, the first observation of a proton transfer from a phenol to a photo-excited Ru polypyridine complex with a proton accepting site.

When PT is followed solely by the non-rate-limiting triplet-singlet deactivation of $\{$**1**(T)-H^+/$PhO^-\}_{IP}$ and back PT sequence, this pathway becomes experimentally indistinguishable from

the physical quenching in the H-bonded **X**(T)-P exciplex that also yields no observable products (Scheme 1 and eq. 1). However, the difference between these pathways appears to be rather trivial, for they both involve either complete or partial proton transfer to **X**(T) bringing about a stronger spin-orbit coupling and the attendant increase of the triplet decay rate to the ground state.

Kinetic solvent effect. Although EPT in an **X**(T)-P exciplex results in the electron going on the Ru center and the proton going on the ligand's N atom, formally this reaction constitutes a hydrogen atom transfer (HAT). For interpreting KSE in HAT, Ingold and co-workers have suggested a straightforward model according to which the H-bonding of an H-atom donor (A-H) to solvent precludes its reaction with an H-atom acceptor, so that only the unbound donor molecules are available for HAT, but the rate constant of the HAT reaction itself is solvent-independent.[16, 18] In other words, the only solvent property that controls the magnitude of KSE in a particular HAT reaction is the solvent's HB basicity. Quantitatively, this model connects the bimolecular HAT rate coefficient in any HB accepting solvent (k_S) with the rate constant for the same reaction (k^0) in a non-HB-accepting solvent (*e.g.*, saturated hydrocarbons or CCl_4) through a simple empirical relationship,

$$log k_S = log k^0 - 8.3\alpha_2^H(\text{A - H})\beta_2^H(\text{S}) \qquad (10)$$

where $\alpha_2^H(\text{A - H})$ and $\beta_2^H(\text{S})$ are Abraham HB acidity of an H-atom donor and solvent's HB basicity, respectively.

Because MeCN is more HB basic than CH_2Cl_2, eq. 10 predicts a linear $log\text{KSE}$ increase with $\alpha_2^H(\text{PhOH})$ for HAT from a phenol; that is,

$$log\text{KSE} = 8.3\left[\beta_2^H(\text{MeCN}) - \beta_2^H(CH_2Cl_2)\right]\alpha_2^H(\text{PhOH}) = 3.24\alpha_2^H(\text{PhOH}) \qquad (11)$$

As shown in Figure 6A for complex **1**, this prediction is contrary to our data that show a decrease of $log\text{KSE}$ with $\alpha_2^H(\text{PhOH})$. A qualitatively similar behavior of KSE is found for complex **2** (Figure S7.1A). Thus, Ingold's model for HAT does not describe KSE in our system. This result is not surprising, however. On the one hand, Figures 6A and S7.1A clearly suggest that we are not dealing with simple atom-to-atom HAT reactions, and, on the other hand, we cannot reasonably expect Ingold's model to apply to concerted EPT. Indeed, this model assumes that the only solvent-dependent factor affecting HAT rates is the H-bonding of the H-donors to solvent, but the rate constant of HAT between an acceptor and H-unbound donor (k^0 in eq. 10) is solvent-independent.

While the latter postulate appears entirely reasonable for simple atom-to-atom HAT that does not involve any appreciable charge redistribution, it is unlikely to hold for EPT with different electron and proton destinations and attendant spatial redistribution of charges. We should, therefore, expect a substantial effect of the solvent's dielectric constant on both the EPT driving force and associated solvent reorganization energy; both factors will make k^0 solvent-dependent and eq. 10 unsuitable for EPT. Our data in Figures 6A and S7.1A attest to this conclusion. In light of this discussion and our data, the recent use of eq. 10 by Mayer, Tolman, and co-workers[66] for converting the EPT rate coefficients measured in THF to those would-be in DMSO and the application of the latter to the free energy correlation analysis appear questionable.

In terms of eqs. 2 and 4, the observed kinetic solvent effect is,

$$\mathrm{KSE} = Const \times \frac{k_q^{app}(CH_2Cl_2)}{k_q^{app}(MeCN)} \times \frac{K_{X\text{-}P}(CH_2Cl_2)}{K_{X\text{-}P}(MeCN)} \times \frac{1 + K_{P\text{-}MeCN}}{1 + K_{P\text{-}CH_2Cl_2}} = \mathrm{KSE}_{cor} \times \frac{1 + K_{P\text{-}MeCN}}{1 + K_{P\text{-}CH_2Cl_2}} \quad (12)$$

where KSE_{cor} is the kinetic solvent effect corrected for the phenol-solvent H-bonding and $Const = (1 + K_{X\text{-}MeCN})/(1 + K_{X\text{-}CH_2Cl_2})$ is an unknown, but phenol-independent factor. The $log\mathrm{KSE}_{cor}$ vs σ_p plot in Figure 6B and Figure S7.1B shows a good linearity for the four phenols that react predominantly through EPT in both solvents, but deviates for cyano- and nitrophenol, which is expected considering the EPT-to-PT modification of the prevailing chemical quenching pathway. The sloping of the $log\mathrm{KSE}_{cor}$ vs σ_p plot together with eq. 12 suggests a solvent effect on k_q^{app} and/or $K_{X\text{-}P}$. Although these factors cannot be experimentally separated, we believe that k_q^{app} is likely to be more strongly modulated by the solvent than $K_{X\text{-}P}$, because the quenching reaction involves a much greater charge redistribution than the H-bonding between **X**(T) and phenol.

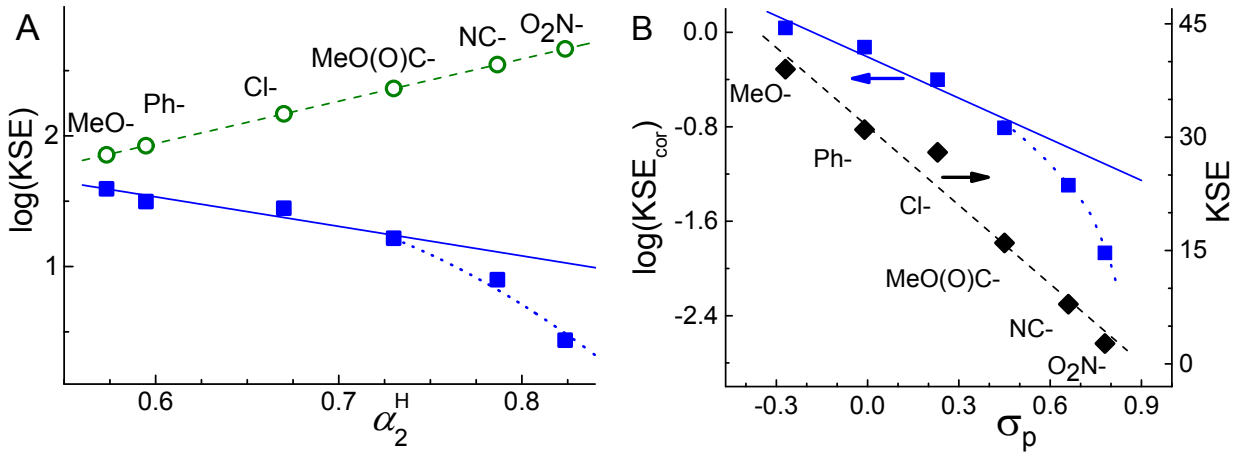

Figure 6. (A) Dependencies of logKSE on phenol's HB acidity for complex **1**: KSE predicted by eq. 11 (circles and dashed line) and observed KSE from Table 1 (squares). (B) Dependencies of $log\mathrm{KSE}_{cor}$ (eq. 12, squares) and observed KSE (diamonds and dashed line showing a linear fit) on σ_p. The solid lines give linear fits through the leftmost 4 data points. The dotted lines serve as the visual aids only. Qualitatively similar patterns are observed for complex **2** (Figure S7.1).

As shown in Figures 6B and S7.1B, the measured KSEs exhibit fair linear correlations with σ_p for both **1** and **2** and all phenols examined here, a peculiar observation that has a certain predictive value, but defies a rational interpretation. Indeed, the linearity transcends the quenching mechanism change embracing not only phenols that react through EPT but also those that engage in PT. Moreover, being by definition thermochemical, the σ_p parameter commonly linearly correlates with logarithms of equilibrium or rate constants, but not with the constants themselves. It will be of interest to examine a wider range of solvents and determine whether the KSE vs σ_p linearity that we observe for MeCN and CH_2Cl_2 is more than just serendipitous.

Conclusions

The bimolecular rate coefficients, k_q^{obs}, for quenching the triplet MLCT excited states, **X**(T), of two Ru polypyridine complexes containing H-bond accepting sites (**1** and **2** in Chart 1) by six *p*-substituted phenols have been measured in CH_2Cl_2 and MeCN and analyzed in terms of a kinetic model that explicitly accounts for the reactants' H-bonding and attendant physical and chemical quenching, as well as for the H-bonding of both reactants to solvent (Scheme 1). While for the less acidic phenols $logk_q^{obs}$ linearly correlates with the Hammett σ_p constant, appreciable deviations from linearity that are indicative of a modification of the quenching mechanism, are observed for the strongly acidic phenols; these deviations occur rather abruptly on the σ_p scale and are particularly large for k_q^{obs} measured in MeCN (Figure 1).

A detailed thermochemical analysis has been conducted and used to discriminate between ET, PT, concerted EPT, and other alternative chemical quenching pathways. This analysis, summarized in Tables 2 and 3, suggests that: (i) The electron transfer from phenols to **X**(T) plays no role in the observed reactivity, and neither do the pathways shown in Scheme 3 and involving concerted or sequential deprotonation of phenols to the solvent; (ii) The most energetically favorable quenching pathway is provided by concerted EPT. However, the thermodynamic advantage of EPT over PT in both solvents is decreasing with phenol's acidity, virtually disappearing for cyano- and nitrophenol in MeCN; (iii) The Hammett σ_p constant is a useful descriptor for analyzing the observed reactivity in terms of free energy correlations, since all phenol's thermochemical properties bearing on the quenching mechanism (H-bonding and Brønsted acidities, O-H bond dissociation free energy, and the phenoxyl radical reduction potential) linearly correlate with σ_p.

Based on the last two observations, the deviations from linearity in the $log k_q^{obs}$ vs σ_p plots have been attributed to a transition of the quenching mechanism from concerted EPT to simple PT; the latter becomes predominant for the most acidic phenols in MeCN, but not in CH_2Cl_2. This conclusion is supported by the magnitudes of the measured and computed PhOH/OD kinetic isotope effects and by the observed reduction of the EPT product yields from **1**(T) upon replacing the weakly acidic *p*-methoxyphenol by the strongly acidic *p*-nitrophenol. This yield decrease is particularly pronounced in MeCN and can be rationalized in terms of the rate-limiting PT within the **1**(T)-nitrophenol H-bonded exciplex followed by rapid triplet deactivation and back PT in the nascent $\{$**1**(T)-$H^+/PhO^-\}_{IP}$ ion pair.

In addition to modulating the relative contribution of the EPT and PT quenching pathways, the solvent strongly affects the bimolecular rate coefficients for the EPT quenching proper (Figure 6). Unlike with the H-atom transfer reactions, this kinetic solvent effect cannot be quantitatively accounted for by the phenol-solvent H-bonding alone, which suggests a solvent effect either on the H-bonding constant between **X**(T) and phenol ($K_{X\cdot P}$ in eq. 2) or, more likely, the unimolecular EPT rate coefficient (k_q^{app} in eq. 4), or both.

Supporting Information

Electronic Supporting Information is available: Kinetic data for reaction between **X**(T) and *p*-substituted phenols; gas-phase and solution thermochemistry of phenols; thermochemistry for the reaction between **X**(T) and phenols; energetics of alternative proton-loss electron transfer mechanisms; computational details for H/D isotope effects; products and yields for reactions of **1**(T) with *p*-methoxy- and *p*-nitrophenol in MeCN and CH_2Cl_2; kinetic solvent effect for complex **2**; coordinates of DFT optimized structures.

Acknowledgements

We are grateful to Drs. Sharon Hammes-Schiffer and Alexander Soudakov for their expert guidance in computing kinetic isotope effects and valuable comments on the draft manuscript, Dr. Koji Tanaka for providing complex **1**, Dr. Jacob Schneider for synthesizing complex **2**, Dr. Norman Sutin for stimulating discussions, and Dr. David Grills for assistance with the manuscript preparation. This work was carried out at Brookhaven National Laboratory and supported by the

U.S. Department of Energy, Office of Science, Office of Basic Energy Sciences, Division of Chemical Sciences, Geosciences, & Biosciences, under contract DE-SC0012704.

References

1. J. Bonin and M. Robert, *Photochem. Photobiol.*, 2011, **87**, 1190-1203.
2. C. C. Hsieh, C. M. Jiang and P. T. Chou, *Acc. Chem. Res.*, 2010, **43**, 1364-1374.
3. S. Hammes-Schiffer, *J. Am. Chem. Soc.*, 2015, **137**, 8860-8871.
4. A. Migliore, N. F. Polizzi, M. J. Therien and D. N. Beratan, *Chem. Rev.*, 2014, **114**, 3381-3465.
5. D. C. Miller, K. T. Tarantino and R. R. Knowles, *Top. Curr. Chem.*, 2016, **374**.
6. J. C. Lennox, D. A. Kurtz, T. Huang and J. L. Dempsey, *ACS Energy Lett.*, 2017, **2**, 1246-1256.
7. S. J. Mora, E. Odella, G. F. Moore, D. Gust, T. A. Moore and A. L. Moore, *Acc. Chem. Res.*, 2018, **51**, 445-453.
8. J. J. Warren, T. A. Tronic and J. M. Mayer, *Chem. Rev.*, 2010, **110**, 6961-7001.
9. D. R. Weinberg, C. J. Gagliardi, J. F. Hull, C. F. Murphy, C. A. Kent, B. C. Westlake, A. Paul, D. H. Ess, D. G. McCafferty and T. J. Meyer, *Chem. Rev.*, 2012, **112**, 4016-4093.
10. O. S. Wenger, *Coord. Chem. Rev.*, 2015, **282**, 150-158.
11. S. V. Lymar, M. Z. Ertem, A. Lewandowska-Andralojc and D. E. Polyansky, *J. Phys. Chem. Lett.*, 2017, **8**, 4043-4048.
12. J. J. Concepcion, M. K. Brennaman, J. R. Deyton, N. V. Lebedeva, M. D. E. Forbes, J. M. Papanikolas and T. J. Meyer, *J. Am. Chem. Soc.*, 2007, **129**, 6968-6969.
13. P. Dongare, A. G. Bonn, S. Maji and L. Hammarström, *J. Phys. Chem. C*, 2017, **121**, 12569-12576.
14. C. Bronner and O. S. Wenger, *J. Phys. Chem. Lett.*, 2012, **3**, 70-74.
15. N. V. Lebedeva, R. D. Schmidt, J. J. Concepcion, M. K. Brennaman, I. N. Stanton, M. J. Therien, T. J. Meyer and M. D. E. Forbes, *J. Phys. Chem. A*, 2011, **115**, 3346-3356.
16. G. Litwinienko and K. U. Ingold, *Acc. Chem. Res.*, 2007, **40**, 222-230.
17. G. Litwinienko and K. U. Ingold, *J. Org. Chem.*, 2003, **68**, 3433-3438.
18. D. W. Snelgrove, J. Lusztyk, J. T. Banks, P. Mulder and K. U. Ingold, *J. Am. Chem. Soc.*, 2001, **123**, 469-477.
19. C. Reichardt, *Solvents and Solvent Effects in Organic Chemistry*, Wiley, 2006.
20. T. Koizumi and K. Tanaka, *Angew. Chem. Int. Ed.*, 2005, **44**, 5891-5894.
21. D. P. Rillema, G. Allen, T. J. Meyer and D. Conrad, *Inorg. Chem.*, 1983, **22**, 1617-1622.
22. D. Polyansky, D. Cabelli, J. T. Muckerman, E. Fujita, T. Koizumi, T. Fukushima, T. Wada and K. Tanaka, *Angew. Chem. Int. Ed.*, 2007, **46**, 4169-4172.
23. Y. Zhao and D. G. Truhlar, *Theor. Chem. Acc.*, 2008, **120**, 215-241.
24. Y. Zhao and D. G. Truhlar, *Acc. Chem. Res.*, 2008, **41**, 157-167.
25. Y. Zhao and D. G. Truhlar, *Rev. Mineral. Geochem.*, 2010, **71**, 19-37.
26. A. V. Marenich, C. J. Cramer and D. G. Truhlar, *J. Phys. Chem. B*, 2009, **113**, 6378-6396.
27. D. Andrae, U. Haussermann, M. Dolg, H. Stoll and H. Preuss, *Theor. Chim. Acta*, 1990, **77**, 123-141.
28. W. J. Here, L. Radom, P. v. R. Schleyer and J. A. Pople, *Ab Initio Molecular Orbital Theory*, Wiley: New York, 1989.
29. M. J. Frisch, G. W. Trucks, H. B. Schlegel, G. E. Scuseria, M. A. Robb, J. R. Cheeseman, G. Scalmani, V. Barone, B. Mennucci, G. A. Petersson, H. Nakatsuji, M. Caricato, X. Li, H. P. Hratchian, A. F. Izmaylov, J. Bloino, G. Zheng, J. L. Sonnenberg, M. Hada, M. Ehara, K. Toyota, R. Fukuda, J. Hasegawa, M. Ishida, T. Nakajima, Y. Honda, O. Kitao, H. Nakai, T. Vreven, J. A. Montgomery, J. E. Peralta, F. Ogliaro, M. Bearpark, J. J. Heyd, E. Brothers, K. N. Kudin, V. N. Staroverov, R. Kobayashi, J. Normand, K. Raghavachari, A. Rendell, J. C. Burant, S. S. Iyengar, J. Tomasi, M. Cossi, N. Rega, J. M. Millam, M. Klene, J. E. Knox, J. B. Cross, V. Bakken, C. Adamo, J. Jaramillo, R. Gomperts, R. E. Stratmann, O. Yazyev, A. J. Austin, R. Cammi, C. Pomelli, J. W. Ochterski, R. L. Martin, K. Morokuma, V. G. Zakrzewski, G. A. Voth, P. Salvador, J. J. Dannenberg,

S. Dapprich, A. D. Daniels, Ö. Farkas, J. B. Foresman, J. V. Ortiz, J. Cioslowski and D. J. Fox, *Gaussian 09, Revision A.02*, Gaussian, Inc., Wallingford, CT, 2010.
30. C. J. Cramer, *Essentials of Computational Chemistry: Theories and Models*, John Wiley & Sons, Chichester, 2nd edn., 2004.
31. F. Weigend and R. Ahlrichs, *Phys. Chem. Chem. Phys.*, 2005, **7**, 3297-3305.
32. S. L. Murov, I. Carmichael and G. L. Hug, *Handbook of Photochemistry*, Marcel Dekker, New York, 2d edn., 1993.
33. K. Izutsu, *Acid-base Dissociation Constants in Dipolar Aprotic Solvents*, Blackwell Scientific Publications, Oxford, First edn., 1990.
34. M. K. Chantooni and I. M. Kolthoff, *J. Phys. Chem.*, 1976, **80**, 1306-1310.
35. M. H. Abraham, P. L. Grellier, D. V. Prior, P. P. Duce, J. J. Morris and P. J. Taylor, *J. Chem. Soc., Perkin Trans. 2*, 1989, 699-711.
36. M. H. Abraham, P. L. Grellier, D. V. Prior, J. J. Morris and P. J. Taylor, *J. Chem. Soc., Perkin Trans. 2*, 1990, 521-529.
37. M. H. Abraham, *Chem. Soc. Rev.*, 1993, **22**, 73-83.
38. Y.-R. Luo, *Comprehensive Handbook of Chemical Bond Energies*, CRC Press, Boca Raton, 2007.
39. R. M. Fuoss, *J. Am. Chem. Soc.*, 1958, **80**, 5059-5061.
40. G. Litwinienko and K. U. Ingold, *J. Org. Chem.*, 2005, **70**, 8982-8990.
41. C. Costentin, M. Robert and J. M. Saveant, *Phys. Chem. Chem. Phys.*, 2010, **12**, 11179-11190.
42. A. V. Makarycheva-Mikhailova, D. M. Stanbury and M. L. McKee, *J. Phys. Chem. B*, 2007, **111**, 6942-6948.
43. N. Song and D. M. Stanbury, *Inorg. Chem.*, 2008, **47**, 11458-11460.
44. V. Y. Shafirovich, S. H. Courtney, N. Q. Ya and N. E. Geacintov, *J. Am. Chem. Soc.*, 1995, **117**, 4920-4929.
45. V. A. Kuzmin, A. Dourandin, V. Shafirovich and N. E. Geacintov, *Phys. Chem. Chem. Phys.*, 2000, **2**, 1531-1535.
46. V. Shafirovich, A. Dourandin and N. E. Geacintov, *J. Phys. Chem. B*, 2001, **105**, 8431-8435.
47. S. Singh and C. N. R. Rao, *Can. J. Chem.*, 1966, **44**, 2611-&.
48. A. Kolbe, *Tetrahedron Lett.*, 1969, 1049-1052.
49. J. W. Boettcher and R. S. Drago, *J. Phys. Chem.*, 1974, **78**, 429-431.
50. M. Simonyi, J. Kardos, I. Fitos, I. Kovacs, S. Holly and J. Pospisil, *Tetrahedron Lett.*, 1975, 565-568.
51. M. Simonyi, I. Kovacs, J. Kardos and S. Holly, *Spectroc. Acta Pt. A-Molec. Biomolec. Spectr.*, 1976, **32**, 1387-1392.
52. M. Rospenk and T. Zeegers-Huyskens, *J. Phys. Chem. A*, 1997, **101**, 8428-8434.
53. Q. Wu and T. Van Voorhis, *Phys. Rev. A*, 2005, **72**, 024502.
54. A. Soudackov and S. Hammes-Schiffer, *J. Chem. Phys.*, 2000, **113**, 2385-2396.
55. S. Hammes-Schiffer, E. Hatcher, H. Ishikita, J. H. Skone and A. V. Soudackov, *Coord. Chem. Rev.*, 2008, **252**, 384-394.
56. S. J. Edwards, A. V. Soudackov and S. Hammes-Schiffer, *J. Phys. Chem. A*, 2009, **113**, 2117-2126.
57. S. Hammes-Schiffer and A. A. Stuchebrukhov, *Chem. Rev.*, 2010, **110**, 6939-6960.
58. B. Auer, L. E. Fernandez and S. Hammes-Schiffer, *J. Am. Chem. Soc.*, 2011, **133**, 8282-8292.
59. S. Horvath, L. E. Fernandez, A. V. Soudackov and S. Hammes-Schiffer, *Proc. Natl. Acad. Sci. U. S. A.*, 2012, **109**, 15663.
60. M. T. Huynh, S. J. Mora, M. Villalba, M. E. Tejeda-Ferrari, P. A. Liddell, B. R. Cherry, A.-L. Teillout, C. W. Machan, C. P. Kubiak, D. Gust, T. A. Moore, S. Hammes-Schiffer and A. L. Moore, *ACS Cent. Sci.*, 2017, **3**, 372-380.
61. D. E. Polyansky, D. Cabelli, J. T. Muckerman, T. Fukushima, K. Tanaka and E. Fujita, *Inorg. Chem.*, 2008, **47**, 3958-3968.

62. P. K. Das, M. V. Encinas, S. Steenken and J. C. Scaiano, *J. Am. Chem. Soc.*, 1981, **103**, 4162-4166.
63. R. J. Crutchley, N. Kress and A. B. P. Lever, *J. Am. Chem. Soc.*, 1983, **105**, 1170-1178.
64. H. Sun and M. Z. Hoffman, *J. Phys. Chem.*, 1993, **97**, 5014-5018.
65. F. Casalboni, Q. G. Mulazzani, C. D. Clark, M. Z. Hoffman, P. L. Orizondo, M. W. Perkovic and D. P. Rillema, *Inorg. Chem.*, 1997, **36**, 2252-2257.
66. D. Dhar, G. M. Yee, T. F. Markle, J. M. Mayer and W. B. Tolman, *Chem. Sci.*, 2017, **8**, 1075-1085.